



AN IMPROVED TECHNIQUE FOR TESTING HELICOPTER ROTOR-PYLON AEROMECHANICAL
STABILITY USING MEASURED ROTOR DYNAMIC IMPEDANCE CHARACTERISTICS

by

Richard L. Bielawa
Associate Professor
Department of Mechanical Engineering,
Aeronautical Engineering & Mechanics
Rensselaer Polytechnic Institute
Troy, New York 12180-3590

TENTH EUROPEAN ROTORCRAFT FORUM
AUGUST 28 – 31, 1984 – THE HAGUE, THE NETHERLANDS

Abstract

The rationale for and theoretical basis of an improved technique for model testing the aeromechanical stability of rotor-pylon coupled rotorcraft systems, are presented. This improved technique is based on the a priori ability to measure experimentally the dynamic impedance characteristics of the isolated (model) rotor in the frequency domain and makes use of the multivariable Nyquist stability criterion. The technique would be especially useful for evaluating helicopter ground and air resonance characteristics of rotorcraft subject to wide variation in pylon characteristics. An especially important and new feature of this test technique is the ability to make quantitative stability assessments of the coupled rotor-pylon system, over and above the quantitative stability assessment afforded by the Nyquist criterion. Formulations include the mathematical eigenproblem for calculating the characteristic loci, the analytic continuation formulae for quantitative stability assessment, the incorporation of hub constraints and the use of scaling laws for combining rotor and pylon characteristics obtained at different scales. Numerical results include comparisons of analytic stability results obtained using both conventional stability eigensolutions and the new rotor impedance matrix method. These results include a preliminary assessment of the impact of hub constraints on stability. The major finding is that, from a theoretical, mathematical viewpoint, the method is practical. The results also give some implications with regard to accuracy requirements to be addressed in the eventual practical measurement of rotor impedance.

1. Introduction

1.1 Background

Of all rotorcraft aeroelastic phenomena presently known, air resonance poses perhaps the greatest challenge to the aeroelastician by virtue of its richness in variety of interacting forces: inertial, aerodynamic, elastic and gravitational.

Air resonance, as a rotorcraft instability phenomenon has received considerable attention in the last fifteen years (Refs.1 through 7) and much is known both qualitatively and quantitatively of its physics. Stated briefly, air resonance is a form of the mechanical instability of rotors known as ground resonance (Ref.8) but one which occurs in flight. The principal features of both ground and air resonance are: (1) the presence of a blade inplane response degree-of-freedom (bending mode or rigid lead-lag motion) characterized by being supercritical (i.e., one whose frequency in the rotating system ω_b is less than rotor rotation frequency Ω), (2) a coincidence or close proximity of the frequency of the regressive, non-rotating coordinate system manifestation of the supercritical blade inplane mode with that of a nonrotating fuselage mode having inplane hub response components ω_f . Stated mathematically: $|(\Omega - \omega_b) - \omega_f| \ll 1$, (3) insufficient internal damping in either or both the blade inplane mode or the fuselage mode. The principal differences between ground and air resonance arise from their respective sources of fuselage stiffness and damping. In ground resonance the sole source of both stiffness and damping is typically the landing gear assembly; in air resonance the sources are multiple: gravity (or alternatively rotor thrust) and the flapwise bending and aerodynamic damping of the rotor blades.

Both types of instability are quite literally "total aircraft" instabilities as opposed to "rotor" instabilities and several disciplines must be brought to bear for their practical stabilization. This is

especially true for air resonance. There now exist several analyses which do reasonable well at predicting the stability characteristics associated with the air resonance phenomenon as validated principally by correlation with model and/or constrained full-scale test results (Refs.3,6,7,9,10).

Yet despite the growing sophistication of these analyses, model air resonance stability tests are still undertaken in the development of new hingeless and bearingless rotor helicopter designs. Note, however, that this heavy reliance on model testing for stability confirmation is not an issue with regard to the related mechanical instability, ground resonance. Typically, existing ground resonance stability analyses are all essentially variants of the classic work of Coleman and Feingold (Ref.8). They are well-accepted as being accurate primary design tools and are routinely used in the design process without experimental confirmation. Experimental confirmation of ground resonance characteristics is generally confined to that which is required on the final manufactured airframe in the certification phase. Thus, a disparity in confidence appears to exist between the analyses for these two very closely related rotor-fuselage coupled instability phenomena. The reason for this disparity is most likely due to the added complexities and, hence, predictive uncertainties brought about by the additional aerodynamic loadings, the internal structural damping and the aeroelastic couplings experienced by the rotor blades in air resonance conditions.

1.2 Existing Model Testing Methodology

As prudent as model testing thus becomes as a backup or complement to whatever air resonance analysis is available, there are nonetheless, distinct intrinsic difficulties with such testing as well. The method typically employed for model scale testing of air resonance stability requires the design and fabrication of a complete, consistently scaled rotor and pylon system. Severe limitations are thereby imposed on the modeling of the pylon structure. The requirement for both Froude and inertia scaling, the available techniques for light weight, low damping model construction, and the need to approximate free-flight with a constrained nonflying pylon all invariably drive the model design to the same simplified pylon configuration: The pylon system is typically designed for articulation only in pitch and roll about some effective center-of-gravity point; the blades are Froude scaled, and the respective masses of the rotor and pylon are appropriately modeled relative to each other. Measuring the stability characteristics of the complete rotor-pylon system is the objective of such model testing, and these characteristics are typically obtained by measuring the transient decay of the responses following some suitably calibrated input disturbance. Use is made either of simple log decrement methods or of more sophisticated data reduction methods (e.g., Ref.11).

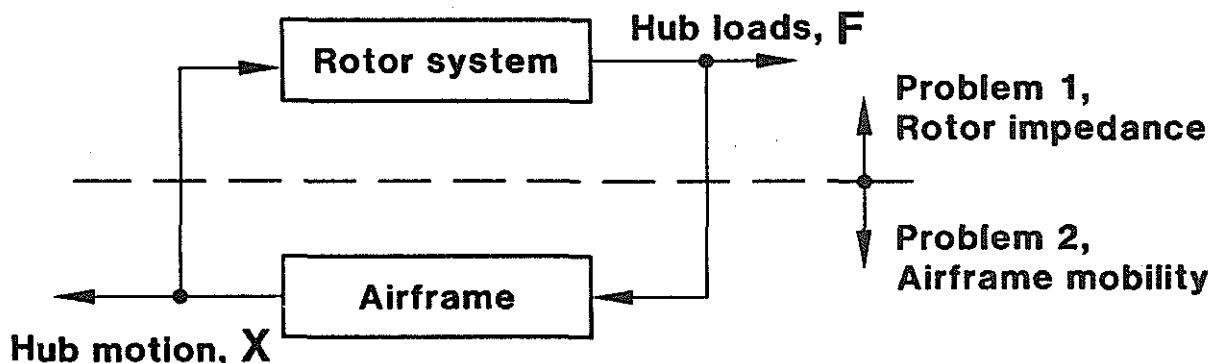
The intrinsic deficiencies in this approach are as follows:

1. Within any test program the requirement to test the combined rotor-pylon system either limits the range of coupling parameters which can be evaluated, or stated alternatively, the test program grows in time and cost to accommodate the testing of many parameter variations. For example, the mass and inertia characteristics of the pylon (helicopter airframe) is subject to considerable variability due to gross weight loading conditions (cargo, passengers, fuel) and external stores. Note, however, that the mass properties of the rotor are relatively constant.

2. The modeling of the pylon mass as a gimbaled rigid body mass articulated in pitch and roll about some effective center-of-gravity point is an approximation of heretofore unknown accuracy. Limited results in the literature of full scale air resonance characteristics in flight (Refs.1,5 and 6) provide scant data with which to make any generalization with regard to the validity of this approximation.
3. Some ranges in pylon parameters may be simply impractical to construct at model scale. This difficulty is compounded by the fact that relative internal damping tends to vary in an inverse manner with model scale. Thus, designing the pylon with sufficiently low internal damping can become a limiting factor.

1.3 New Test Methodology

An improved method for testing the rotor-pylon coupled aeromechanical stability characteristics of model rotor systems forms the subject of the present paper. This method forms a radical departure from traditional methods and is based on assessing the appropriate dynamics of the two component subsystems, the rotor and the pylon, separately. As shown in Fig.1 the rotorcraft can be conceptualized as being comprised of two dynamic subsystems each of which interacts at their mutual attachment point, the rotor hub. The rotor system generates hub loads in response to the hub



- **Problem 1: $[F/X]$, difficult to calculate, use test**
- **Problem 2: $[X/F]$, wide variation, easier to calculate, use analysis**

Figure 1 Conceptualization of Rotor-Airframe Dynamic Interactions

motion (rotor impedance), and the airframe generates hub motion in response to hub loads from rotor (airframe mobility). Rotor impedance is generally more difficult to calculate, but is less subject to wide variation in many parameters and, hence, is most appropriate for test evaluation. Pylon mobility, however, is subject to wide variability, but is far easier to calculate accurately than to test at model scale. This approach to system modeling, wherein the rotor and pylon subsystems are considered separately, and the advantages for doing so have already been recognized with regard to the analysis of vibration relating to rotor-pylon interaction (Ref.12).

The improved stability test methodology is accordingly based on the following points:

1. The rotor alone shall be tested for dynamic characteristics in all five degrees-of-freedom (three translations, pitch and roll) to measure its aeromechanical impedance for each operating condition. A frequency dependent matrix description will ensue.
2. The airframe mobility characteristics, as defined by a frequency dependent matrix (again, degrees-of-freedom in three translations, pitch and roll) but with all appropriate parameter variations, shall be provided by some other source. Such sources could include an analytic calculation of any desired complexity using finite element techniques (e.g., NASTRAN et al.) or even full scale or model scale experimentation.
3. The two dynamic descriptions are then combined in an eigen-solution technique, as described below, to assess the stability characteristics of the complete system.

It should be pointed out that such testing of either of these two helicopter subsystems is not of itself new. Reference [13] describes work done in measuring the aeromechanical impedance of an isolated rotating model helicopter rotor. Similarly, it is common practice to measure the impedance characteristics of the helicopter airframe (without the rotor) to ascertain equivalent masses, damping and natural frequencies for subsequent inclusion in calculations of full-scale ground resonance characteristics. But these two types of subsystem testing have not been directed to any identifiable alternate, more productive use of models for testing rotor-pylon coupled aeromechanical instabilities. The missing technology, heretofore, has been the unifying principles which, when taken with the impedance mobility characteristics of the two subsystems, yield stability information of the combined system.

The development of these unifying principles constitutes the substance of this paper. The paper does not address the problem of how to measure rotor impedance, but rather, if rotor impedance measurements were available, of what advantageous use could be made of them. The actual test methodology required to measure rotor impedance still needs further development beyond the pioneering work of Ref.[13]. The description of that development effort, however, must form the subject of future reporting.

The remainder of this paper presents first the theoretical development for the unifying principles which enable the assessment of combined system stability. These principles allow not only the attainment of stability boundaries, but also of qualitative approximations of the actual stability levels. Second, numerical results are presented for both ground resonance and air resonance applications which demonstrate the theory. These results furthermore provide a quantitative assessment of the inaccuracies posed by the constraints on airframe articulation inherent in a pitch-roll gimbal retention.

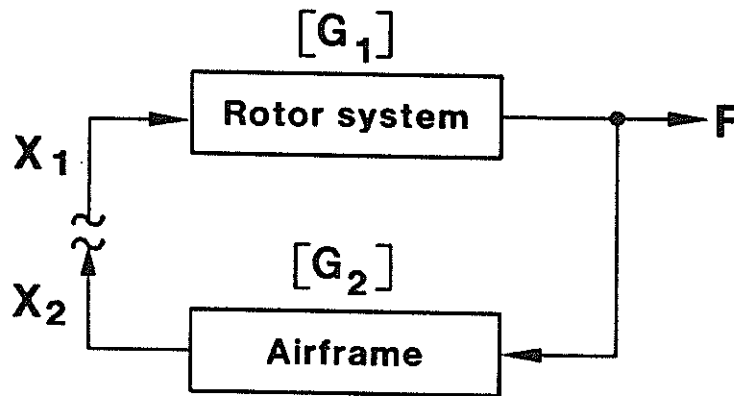
2. Theoretical Development

2.1 Multivariable Nyquist Stability Criterion

The familiar, classic Nyquist stability criterion, as formulated for single variable dynamic feedback systems, is over 50 years old and

well-established as a standard control system design tool (e.g., Ref.14). Extension of the basic concept to multivariable feedback systems, however, has occurred only relatively recently (Ref.15, 1977). As developed in this latter reference the formulations are mathematically rigorous and intended for a wide general class of feedback systems application. A full exposition of this formulation and a formal application of it to the problem at hand appears unwarranted as a more direct, perhaps more heuristic approach has been found to work quite well, nonetheless.

The starting point used in both the present and Ref.[15] formulations is the mathematical conceptualization of the loop closure between the two subsystems. As shown in Fig.2 the two frequency dependent ($N \times N$) dynamic matrices G_1 , representing rotor impedance, and G_2 , representing airframe mobility, are mathematically combined by generalizing the closure condition at a point in the feedback loop. As shown, the feedback is deliberately cut and the system responses are then assumed to be undamped sinusoidal rather than the damped (or divergent) sinusoidal as would be obtained with



$$\{F\} = [G_1] \{X_1\}; \text{ Rotor impedance-from test}$$

$$\{X_2\} = [G_2] \{F\}; \text{ Airframe mobility-from analysis}$$

$$\{X_2\} = \Lambda \{X_1\}; \text{ Loop closure}$$

Figure 2 Basis for Multivariable Nyquist Criterion - Characteristic Loci Eigenvalue Problem

actual loop closure. Three simple relationships define the closure condition.

Rotor impedance:

$$\{F\} = [G_1(\omega)] \{X_1\} \quad (1)$$

Airframe mobility:

$$\{X_2\} = [G_2(\omega)] \{F\} \quad (2)$$

Conditions across loop closure:

$$\{X_2\} = \Lambda \{X_1\} \quad (3)$$

Equation (3) implements the mandate that the (acceleration) responses at the end of the opened loop X_2 shall be proportional to those at the start of the loop X_1 . The undetermined constant of proportionality Λ at this point is allowed to be arbitrary and complex-valued.

Taken together the above frequency dependent matrix equations define an $(N \times N)$ eigenvalue problem:

$$[G_2(\omega)] [G_1(\omega)] \{X_1\} = \Lambda(\omega) \{X_1\} \quad (4)$$

where the N frequency dependent eigenvalues $\Lambda(\omega)$ are denoted the characteristic loci.

As applied to the present problem, the multivariable Nyquist criterion can be simply stated that the combined system (with loop closure) shall be unstable if any of the characteristic loci Λ_n cross the real axis in the complex plane at a point greater than unity, $(+1 + i0)$.

The proof presented herein is essentially a heuristic one: If one of the characteristic loci Λ_n is exactly equal to unity, then complete closure is in fact restored and, for sinusoidal motion the restored system is, by definition, neutrally stable. If Λ_n is again strictly real, but greater in magnitude than unity, then the responses are "in phase" across the cut, but growing in amplitude, i.e., unstable. Similarly, if Λ_n is real, but less than unity the system must be correspondingly stable.

Viewed another way, the real axis crossing point of each of the characteristic loci provides a measure of the system's ability to increase its energy in each mode, respectively, in accordance with the autogenous growth (or decay) of the responses upon each turn around the feedback loop. As developed for both single and multivariable feedback systems (Refs. 14 and 15) the Nyquist criterion is canonically stated more generally in terms of the number of clockwise encirclements of a critical point (either +1 or -1, depending on positive or negative feedback) by the ratio of open-loop output to input (Λ in the present case), and the number of unstable poles of the open-loop system. The present formulation is seen to be compatible with this more usual statement of the Nyquist criterion by first noting that any encirclement of the +1 point requires Λ to cross the real axis at a value greater than unity and secondly by assuming that the open loop transfer function $[G_2][G_1]$ typically is stable. That is, the hub-fixed rotor, by itself, is assumed to be stable as is the rotorless airframe by itself. In effect, the canonically stated Nyquist criterion equates the number of system unstable poles arising only due to the feedback loop closure to the number of encirclements of +1 (or -1, as appropriate), which is essentially what is put forth herein.

It needs to be stressed that the usefulness of the multivariable Nyquist stability criterion lies in the resulting ability to separate out the dynamics of the rotor from those of the airframe and deal with each separately. The $[G_1]$ and $[G_2]$ matrices of Eqs. (1) and (2) can be obtained from different sources and at different scales and yet still be combined, as is described in a subsequent section. Thus, the $[G_1]$ rotor impedance matrix only need be obtained experimentally at model scale.

2.2 Quantitative Stability Characteristics

As useful as the above-formulated Nyquist technique is, it can only in of itself give stability boundaries. Usually, more precise knowledge

of stability is required, as quantified either by critical damping ratio, characteristic exponent or stability margin (with respect to some parameter such as gain or phase). The development to follow presents a method for estimating the characteristic exponents from the variations of the characteristic loci when in close proximity to the critical $(+1+i0)$ point. Essentially the method is a straightforward application of analytic continuation of a complex variable.

Let us begin the formulation by writing the Equation (4) eigenproblem in a more general form:

$$\left[\Lambda(\lambda) - [G_2(\lambda)][G_1(\lambda)] \right] \{X_1\} = 0 \quad (5)$$

where the frequency is now generalized to be of the Laplace variable domain form:

$$\lambda = \sigma + i\omega \quad (6)$$

and where each of the characteristic loci is now a complex-valued (analytic) function of the complex frequency:

$$\Lambda(\lambda) = \Lambda_R(\lambda) + i\Lambda_I(\lambda) \quad (7)$$

The objective is to closely approximate the characteristic exponent σ in Eq.(6) knowing the behavior of Λ as a function of ω near the critical point. Note first that in the frequency domain, as noted earlier, $\Lambda(\omega)$ will have a value of $1 + \epsilon$ (where ϵ is a known small number) at the real axis crossing frequency $\omega = \hat{\omega}$ (also known). In the Laplace variable domain, however, $\Lambda(\lambda)$ has the value of 1 exactly at the value of λ which we seek, (which is another way of stating the classic stability eigenproblem). Assuming that $\Lambda(\lambda)$ is an analytic function in the neighborhood of $(1+i0)$, we can expand Λ in a Taylor series taking the derivatives in the frequency (imaginary) axis direction and evaluating them at the point $\hat{\lambda} = i\hat{\omega}$:

$$\Lambda(\lambda) = \Lambda(\hat{\lambda}) + (\lambda - \hat{\lambda}) \frac{d\Lambda}{d\lambda}(\hat{\lambda}) + \frac{1}{2} (\lambda - \hat{\lambda})^2 \frac{d^2\Lambda}{d\lambda^2}(\hat{\lambda}) + \dots \quad (8)$$

Since:

$$\frac{d\Lambda}{d\lambda} = \frac{d\Lambda_R}{d(i\omega)} + i \frac{d\Lambda_I}{d(i\omega)} = \frac{d\Lambda_I}{d\omega} - i \frac{d\Lambda_R}{d\omega} \quad (9a)$$

$$\frac{d^2\Lambda}{d\lambda^2} = \frac{d}{d(i\omega)} \left(\frac{d\Lambda}{d(i\omega)} \right) = - \frac{d^2\Lambda_R}{d\omega^2} - i \frac{d^2\Lambda_I}{d\omega^2} \quad (9b)$$

$$(\lambda - \hat{\lambda}) = \sigma + i\Delta\omega \quad (9c)$$

where

$$\Delta\omega = \omega - \hat{\omega} \quad (9d)$$

and upon neglecting the second order and higher order terms in Eq.(8), a simple equation results for σ and $\Delta\omega$:

$$\Lambda(\lambda) = 1 = 1 + \epsilon + \left(\frac{d\Lambda_I}{d\omega} - i \frac{d\Lambda_R}{d\omega} \right) (\sigma + i\Delta\omega) \quad (10)$$

which reduces to two real simultaneous equations:

$$\left(\frac{d\Lambda_I}{d\omega}\right) \sigma + \left(\frac{d\Lambda_R}{d\omega}\right) \Delta\omega = -\epsilon \quad (11a)$$

$$-\left(\frac{d\Lambda_R}{d\omega}\right) \sigma + \left(\frac{d\Lambda_I}{d\omega}\right) \Delta\omega = 0 \quad (11b)$$

which can be readily solved to yield:

$$\sigma = \frac{-(d\Lambda_I/d\omega) \epsilon}{(d\Lambda_I/d\omega)^2 + (d\Lambda_R/d\omega)^2} \quad (12a)$$

$$\omega = \hat{\omega} - \frac{(d\Lambda_R/d\omega) \epsilon}{(d\Lambda_I/d\omega)^2 + (d\Lambda_R/d\omega)^2} \quad (12b)$$

Note that the small number ϵ , (the increment beyond the critical point +1 that the characteristic locus crosses the real axis), the frequency at the crossing point $\hat{\omega}$, as well as the derivatives of Λ_R and Λ_I contained in the above equations are all obtainable numerically from the calculations for the characteristic loci.

A more accurate estimate of the damping σ and flutter frequency ω can be obtained by retaining the second derivative term in Eq.(8):

$$\frac{1}{2} \frac{d^2\Lambda}{d(i\omega)^2} (\lambda - \hat{\lambda})^2 + \frac{d\Lambda}{d(i\omega)} (\lambda - \hat{\lambda}) + \epsilon = 0 \quad (13)$$

Solution of Eq.(13) for σ and $\Delta\omega$ is perhaps best done using the binomial theorem on a computer with complex arithmetic, and no attempt is made here to provide a closed form solution similar to Eqs.(12a) and (12b). It is sufficient to note that the general methodology for obtaining accurate values of σ and $\Delta\omega$ is limited only by the closeness of the real axis crossing to the critical point, the accuracy in numerically estimating the various derivatives of Λ , and the degree to which the Taylor series expansion is taken.

The above material forms the heart of the theoretical development required for the use of impedance matrices for stability assessment. Two additional related topics are treated in this main section in anticipation of results to be presented in a subsequent section. The first relates to the modifications of the rotor impedance and pylon mobility matrices due to hub constraints. The second relates to the use of scaling techniques for the combining of results for rotor impedance and pylon mobility which were respectively obtained at different scales.

2.3 Hub Constraints

This section deals with the modifications of the rotor impedance and pylon mobility matrices resulting from constraints imposed on the hub motion. In particular, the material is addressed to a validity assessment of the use of a gimbal mount to constrain the pylon mass in typical combined rotor-pylon model testing.

A simple generalized statement of the hub constraint is afforded using a constraint matrix [C]:

Responses:

$$\{X\} = [C] \{\tilde{X}\} \quad (14a)$$

Loads:

$$\{\tilde{F}\} = [C]^T \{F\} \quad (14b)$$

where the $[C]$ matrix is typically nonsquare and the $\{\tilde{\cdot}\}$ denoted vectors have a reduced number of components due to constraining.

a) Rotor Impedance. The usual statement of rotor impedance, Eq.(1) can be combined with Eqs.(14a) and (14b) as follows:

$$\begin{aligned} \{F\} &= [G_1] \{X\} = [G_1] [C] \{\tilde{X}\} \\ \{\tilde{F}\} &= [C]^T \{F\} = [C]^T [G_1] [C] \{\tilde{X}\} \end{aligned} \quad (15)$$

Thus, the constrained impedance matrix becomes:

$$[\tilde{G}_1] = [C]^T [G_1] [C] \quad (16)$$

b) Pylon Mobility. The pylon mobility matrix, Eq.(2), can best be constrained by first converting it to an impedance matrix and then inverting the final result:

$$\{X\} = [G_2] \{F\} \rightarrow \{F\} = [G_2]^{-1} \{X\} \quad (17)$$

Thus:

$$\{\tilde{F}\} = [C]^T [G_2]^{-1} [C] \{\tilde{X}\} \quad (18a)$$

or

$$\{\tilde{X}\} = \left[[C]^T [G_2]^{-1} [C] \right]^{-1} \{\tilde{F}\} \quad (18b)$$

$$\therefore [\tilde{G}_2] = \left[[C]^T [G_2]^{-1} [C] \right]^{-1} \quad (19)$$

2.4 Scaling Techniques

The objective of using scale model testing at all is to be able to relate the results quantitatively to the full-scale situation. Assuming the use of Froude scaling, Ref.[16] provides the means for converting an impedance matrix measured at model-scale $[G_1]_{MS}$ to one appropriate to full-scale. The measured impedance matrix pertains to model-scale loads and accelerations:

$$\{F\}_{MS} = [G_1]_{MS} \{\ddot{Z}\}_{MS} \quad (20)$$

where

$$\{F\} = [F_x, F_y, F_z, M_x, M_y] \quad (21a)$$

$$\{\ddot{Z}\} = [\ddot{x}, \ddot{y}, \ddot{z}, \ddot{\theta}_x, \ddot{\theta}_y] \quad (21b)$$

Then, the load and acceleration vectors $\{F\}$ and $\{\ddot{Z}_1\}$ can respectively be scaled using the length scale factor λ_ℓ as follows:

$$\{F\}_{FS} = \begin{bmatrix} \lambda_\ell^{-3} & & & & & \\ & \lambda_\ell^{-3} & & & & \\ & & \lambda_\ell^{-3} & & & \\ & & & \lambda_\ell^{-4} & & \\ & & & & \lambda_\ell^{-4} & \\ 0 & & & & & \lambda_\ell^{-4} \end{bmatrix} \{F\}_{MS} \quad (22)$$

$$= [T_F] \{F\}_{MS}$$

$$\{\ddot{Z}\}_{MS} = \begin{bmatrix} 1 & & & & & \\ & 1 & & & & \\ & & 1 & & & \\ & & & \lambda_\ell^{-1} & & \\ & & & & \lambda_\ell^{-1} & \\ 0 & & & & & \lambda_\ell^{-1} \end{bmatrix} \{\ddot{Z}\}_{FS} \quad (23)$$

$$= [T_{\ddot{Z}}] \{\ddot{Z}\}_{FS}$$

Thus, the full-scale impedance matrix is given by:

$$[G_1]_{FS} = [T_F] [G_1]_{MS} [T_{\ddot{Z}}] \quad (24)$$

where

$$\lambda_\ell = \ell_{MS} / \ell_{FS}$$

is the model scale factor.

3. Numerical Results

As is noted above, the thrust of this paper is to show the advantages of conducting rotor-pylon aeromechanical stability experimentation using measured rotor impedance matrices, once they should be available. Since detailed experimentally obtained impedance matrices are not yet generally available, the potential of this new test methodology must be demonstrated by some other means. Thus, in lieu of actual experimentally measured rotor impedance matrices, analytically derived ones were calculated based on simplified equations of motion appropriate for both helicopter ground and air resonance.

The dynamic equations used for this purpose are given in Appendix A. These equations can be used either for ground resonance calculations [Eqs. (A.1a, b, e, f), with $\bar{\theta}_{x_f} = \bar{\theta}_{y_f} = \bar{\theta}_{x_r} = \bar{\theta}_{y_r} = 0$], or for air resonance in their complete form, except with $K_{f_x} = K_{f_y} = 0$. It should be stressed that these equations are not put forth with the intention of providing the reader with yet another "more accurate" modeling of air resonance characteristics for design purposes. Rather they are used only as a reasonably representative mathematical approximation of helicopter air resonance characteristics, strictly for the purpose of demonstrating the theory put forth in this paper.

In addition to providing an approximation to the rotor impedance and pylon mobility matrices, the use of analysis provides an excellent check of the validity of the impedance stability assessment technique. The stability predictions afforded by the impedance technique can be directly compared with those obtained using the usual Laplace variable eigensolution of the entire system [Eqs. (A.1a-f)]. For both the ground resonance and air resonance numerical results the same four-bladed model hingeless rotor configuration was used. Table 1 lists the mechanical and geometrical properties of both the selected blade configuration as well as the nominal pylon/airframe configuration.

TABLE 1
AEROMECHANICAL PROPERTIES OF ROTOR AND PYLONS USED
IN NUMERICAL EXAMPLES

1. Rotor Properties	
(Nominal) tip speed, ΩR	90.50 m/s
Froude number @ nom ΩR	608.41
Radius, R	1.37 m
Mass distribution, m'	4.98 kg/m
Flatwise bending stiffness, EI_w	1.904 Nm ²
Edgewise bending stiffness, EI_v	106.65 Nm ²
(Nominal) modal damping, ζ_v, ζ_w	0.005
Number of blades, b	4
2. Ground Resonance Pylon Properties	
x-direction: Mass, m_{f_x}	18.97 kg
Frequency, ω_{f_x}	16.0 rad/s
Damping ratio, ζ_{f_x}	0.2
y-direction: Mass, m_{f_y}	11.68 kg
Frequency, ω_{f_y}	28.0 rad/s
Damping ratio, ζ_{f_y}	0.1
3. Supplementary Rotor Properties (Air Resonance Cases)	
Lock number, γ	5.854
C_T/σ (hover)	0.075
Chord, c	11.65 cm
Precone angle, β_B	0.5 deg
Collective angle, $\theta_{.75R}$	9.98 deg
Inflow, λ	-0.06371
a	0.1/deg
c_{d_o}	0.008
Thrust, T	387.20 N
4. Air Resonance Pylon Properties	
Pylon mass, m_f	37.02 kg
c.g. location, h_1	0.305 m
(Nominal) roll inertia, I_{ϕ_f}	0.163 kg-m ²
(Nominal) pitch inertia, I_{θ_f}	0.746 kg-m ²

3.1 Analytical Impedance and Mobility Matrices

The required rotor impedance and pylon mobility matrices can be obtained from the eigensolution equations of motion in the following steps:

- 1) Establish sinusoidal motion responses by setting $\lambda = i\omega$. Thus,

$$[A]\lambda^2 + [B]\lambda + [C] \{\bar{Z}\} = 0$$

becomes:

$$[H_R(\omega)] + i[H_I(\omega)] \{\bar{Z}\} = 0 \quad (25)$$

- 2) Partition the dynamic matrices according to rotor, pylon forces and motion:

$$\begin{array}{l}
 \text{pylon forces} \\
 \text{rotor forces}
 \end{array}
 \left\{ \begin{array}{c}
 \left[\begin{array}{cc}
 H_{11}^{(P)} + H_{11}^{(R)} & H_{12} \\
 \hline
 H_{21} & H_{22}
 \end{array} \right] \begin{Bmatrix} \bar{Z}_p \\ \bar{Z}_b \end{Bmatrix} \\
 \underbrace{\hspace{10em}}_{\text{pylon motion}} \quad \underbrace{\hspace{10em}}_{\text{blade motion}}
 \end{array} \right\} \quad (26)$$

Note that the H_{11} submatrix represents forces arising from both pylon and rotor sources, $H_{11}^{(P)}$ and $H_{11}^{(R)}$, respectively.

- 3) Using the basic definitions for rotor impedance and pylon mobility, Eqs.(1) and (2), form the required matrices from Eq.(26):

Pylon mobility is determined by considering the pylon force excitation arising from pylon motion of pylon mass elements.

Thus:

$$[G_2(\omega)] = [H_{11}^{(P)}]^{-1} \quad (27)$$

Rotor impedance is determined by considering the pylon force excitations $\{F_p\}$ arising from hub and elastic blade motions of the rotor mass elements:

$$\{F_p\} = - [H_{11}^{(R)}] \{\bar{Z}_p\} - [H_{12}] \{\bar{Z}_b\} \quad (28)$$

where

$$\{\bar{Z}_b\} = - [H_{22}]^{-1} [H_{21}] \{\bar{Z}_p\} \quad (29)$$

Thus:

$$[G_1(\omega)] = [H_{12}] [H_{22}]^{-1} [H_{21}] - [H_{11}^{(R)}] \quad (30)$$

3.2 Ground Resonance Results

A basic four degree-of-freedom equation set was used to define the ground resonance characteristics [Eqs. (A.1a,b,e,f) in Appendix A]. This equation set defines the coupled dynamics involving two hub (translation) degrees-of-freedom, x_p and y_p , and two rotor mode blade edgewise deflection variables, e_x and e_y . The results of the stability eigensolution for the nominal rotor and pylon configurations with varying rotor speed are given in Fig.3. Specifically, this figure shows the variations in damping and

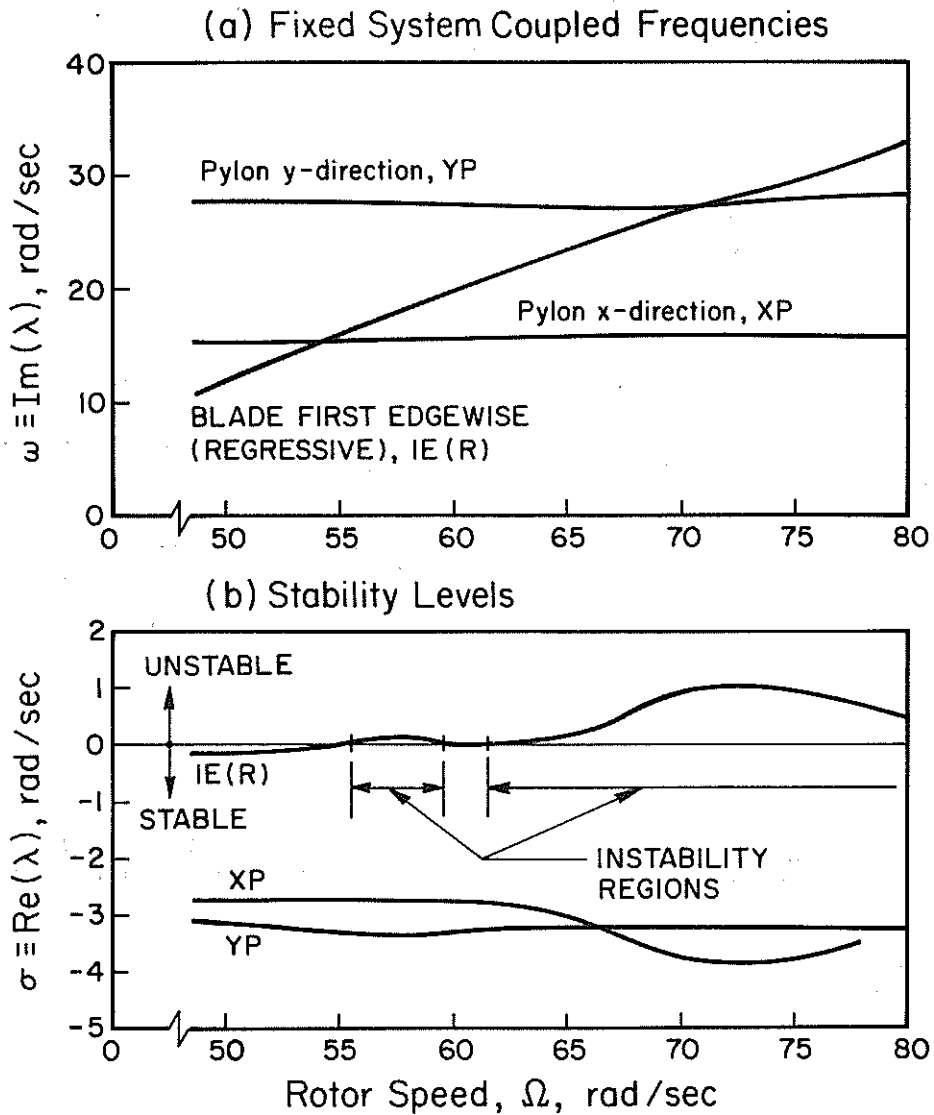


Figure 3 Stability Eigenvalue Variation with Rotor Speed for Nominal Ground Resonance Configuration

coupled frequency for the three principal coupled modes of response: pylon x- and y-dominant hub translation, and the blade regressive edgewise dominant deflections, with rotor speed. Note that the blade advancing edgewise dominant mode is of much higher frequency, well-damped and of no importance to the ground resonance instability characteristics. In all subsequent discussion of results, this mode is omitted for clarity. Figure 3 clearly shows the classic ground resonance instability regions centered at rotor speeds of $\Omega = 57$ and 72 rad/sec for the nominal pylon configuration. These results, wherein an instability region results at each of the intersections of the blade regressive edgewise mode with a pylon mode, are typical of the ground resonance instability.

For the remainder of the discussion of ground resonance results, conditions only within the higher rotor speed instability region ($\Omega = 65$ rad/sec) were selected. At this rotor speed the eight eigenvalues (stability roots) were calculated to be:

$$\lambda_{1,2} = -0.712 \pm i 115.017$$

$$\lambda_{3,4} = -2.968 \pm i 27.041$$

$$\lambda_{5,6} = +0.152 \pm i 23.569$$

$$\lambda_{7,8} = -3.262 \pm i 15.704.$$

Using Eq.(30) the elements of a pseudo-rotor impedance matrix G_1 were calculated varying the oscillation frequency ω . This pseudo-rotor impedance matrix is so denoted because, for the relatively simple case of ground resonance, the $H_{11}^{(P)}$ and $H_{11}^{(R)}$ terms were not separated out, the $H_{11}^{(R)}$ terms being retained instead in the G_2 matrix calculations. The variations of the four elements of the G_1 matrix with frequency are shown in Fig.4. Note that the G_1 matrix for ground resonance is skew-symmetric. Because of this skew-symmetry and rotor isotropy only two numerically distinct values result. Note also that these two values are approximately 90 degrees apart in phase, but both have their greatest variability in the same frequency range ($\omega = 23 \rightarrow 24$ rad/sec) and a local maximum at the same frequency ($\omega = 23.4$ rad/sec). Furthermore, both numerical values have zero values for $\omega = 0$, tend to ∞ as $\omega \rightarrow \infty$ and undergo a total phase shift of 180° .

Using the rotor impedance matrix results together with a similarly calculated pylon mobility matrix [Eq.(27)], the characteristic loci were obtained for the coupled rotor-ptylon system. The variations of these characteristic loci with frequency are shown in Fig.5 for the nominal configuration ($\zeta = 0.005$) and for an augmented damping configuration ($\zeta = 0.010$). The figure clearly shows the enclosure of the critical point ($1+i0$) by one of the two characteristic loci for the nominal configuration, and a non-enclosure for the augmented damping case.

Estimations of the actual frequencies of real axis crossing, as well as of the derivatives of the characteristic loci, Eqs.(9a) and (9b), were obtained by use of Lagrangian interpolation polynomials, Ref.[17]. For each of the components of the characteristic loci (real and imaginary) four numerical values were used, two on each side of the real axis to form cubic polynomial fits of the calculated results. Solution for the real axis crossing was then achieved by solving for the value of ω for which the imaginary part is zero. Use of this frequency together with the Lagrangian interpolation polynomials then enabled a direct calculation of the derivatives.

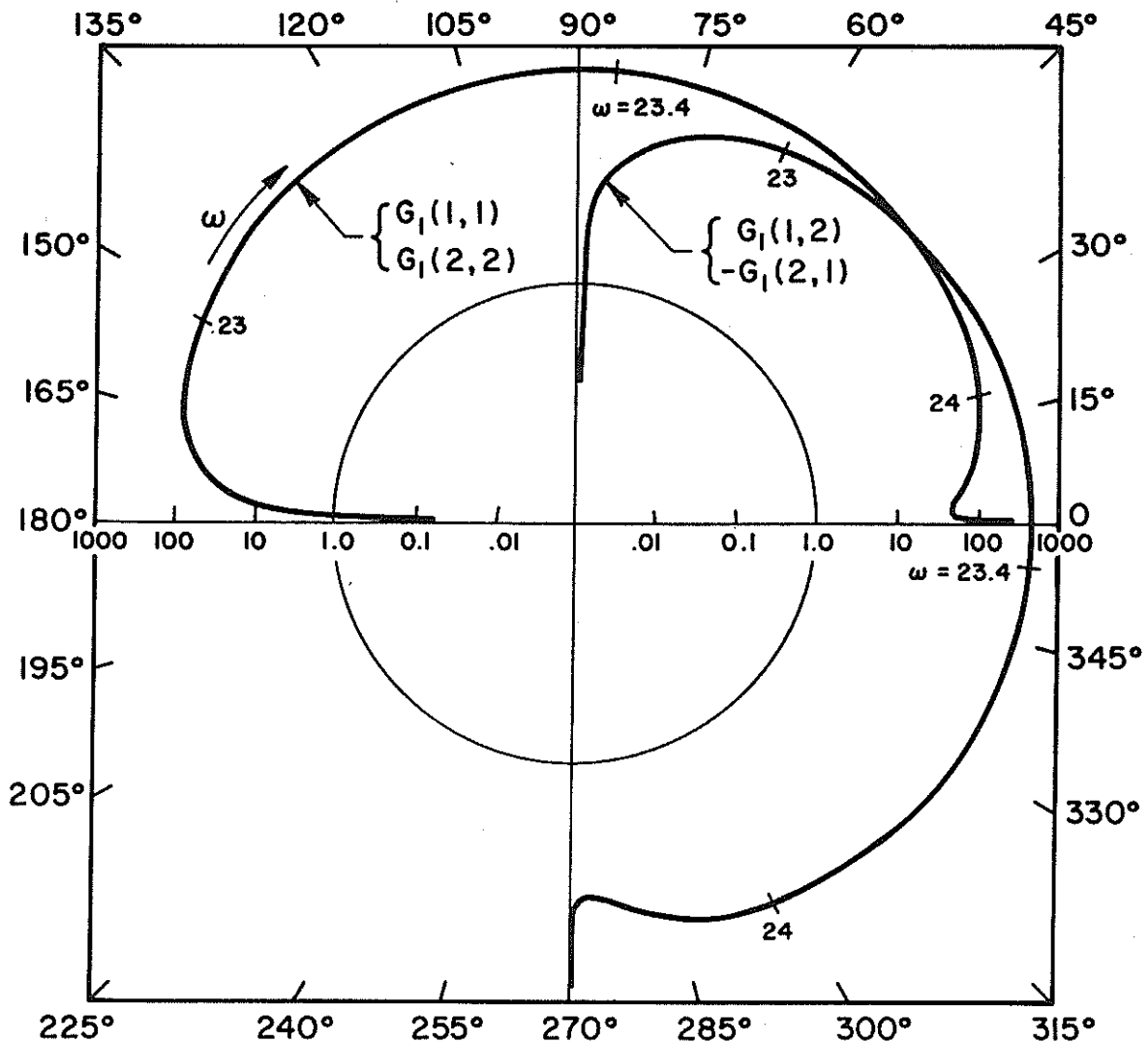
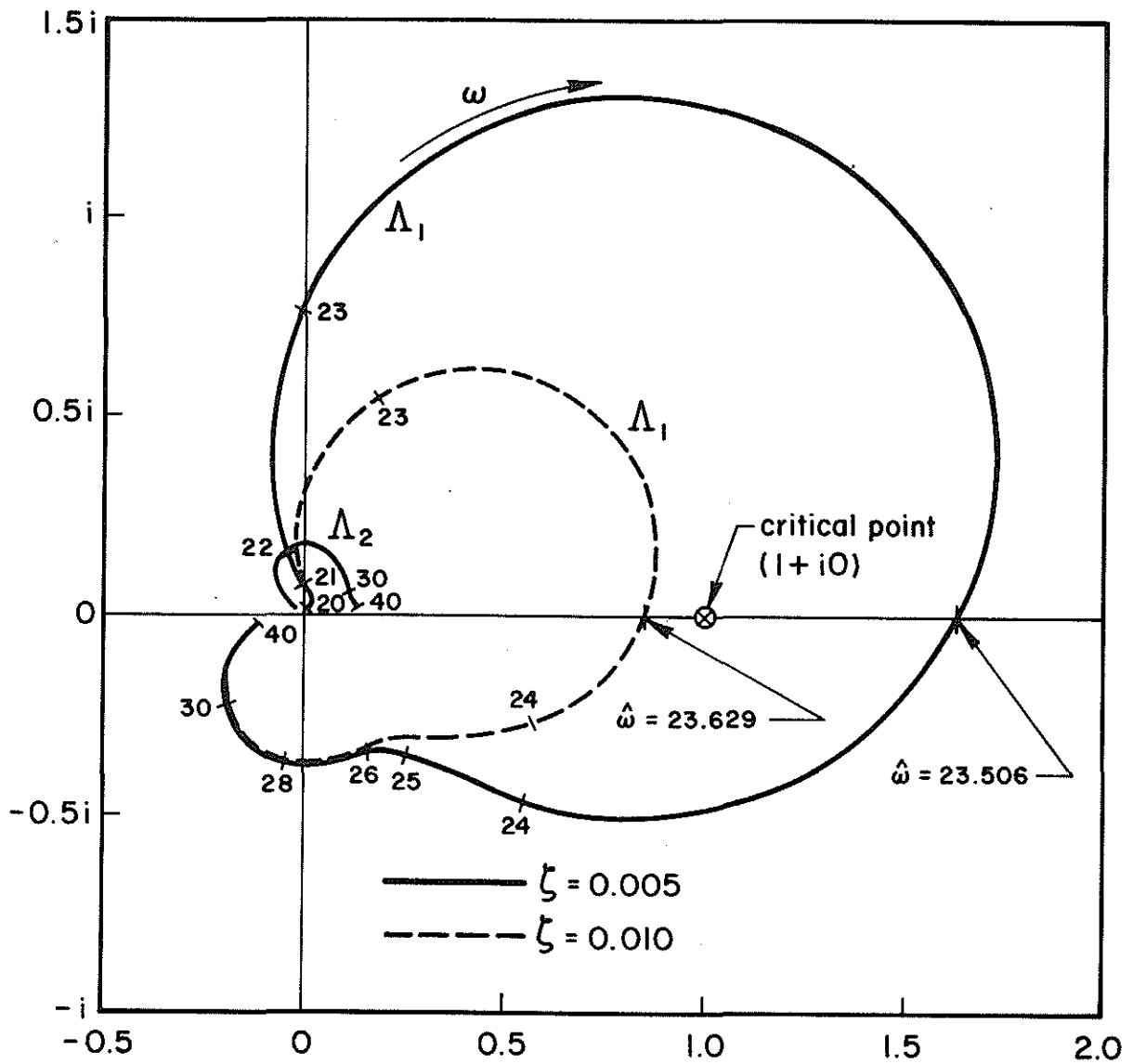


Figure 4 Variation of Elements of Rotor Impedance Matrix with Frequency, $\Omega = 65$ rad/sec, Ground Resonance Case

Using these numerical techniques the characteristic locus for the nominal configuration was found to cross the real axis at a critical frequency $\hat{\omega}$ of 23.506 rad/sec compared with the pylon uncoupled x- and y-direction frequencies of 16.0 and 28 rad/sec, respectively, and the actual coupled ground resonance frequency of 23.569 rad/sec, i.e., $\text{Im}(\lambda_{5,6})$.

Combining the numerical results used to generate Fig.5, together with the formulations given in the above section on quantitative stability characteristics, provides estimates of the critical system eigenvalues. For the nominal and augmented damping configurations these calculations and respective percent errors are summarized in Table 2.

These results clearly show the ability of the analytic construction scheme to yield reasonably accurate estimates of the ground resonance instability eigenvalues. Not unexpectedly, the estimates improve with higher order approximation.



.Figure 5 Variations of Characteristic Loci for Ground Resonance Condition of Instability, $\Omega = 65.0$ rad/sec, Nominal and Augmented Damping Cases

TABLE 2
EIGENVALUE ESTIMATES (GROUND RESONANCE)

Condition	$\sigma, \text{Re}(\lambda)$		$\omega, \text{Im}(\lambda)$	
	Value	% Error	Value	% Error
1. Nominal Configuration				
• Actual eigenvalue	0.152	-	23.569	-
• First order [Eq.(2)]	0.088	42.1	23.549	0.08
• Second order [Eq.(3)]	0.146	3.9	23.477	0.39
2. Augmented Damping Configuration				
• Actual eigenvalue	-0.0724	-	23.599	-
• First order approx.	-0.0870	13.5	23.596	< 0.1
• Second order approx.	-0.0740	2.2	23.600	< 0.1

3.3 Air Resonance Results

Similar to the procedure used for the ground resonance results, the equation set presented in Appendix A was used. For the air resonance calculations, however, the full complement of eight dynamic equations was utilized and the aerodynamic terms and Coriolis terms arising from precone were activated. The principal modes of interest for the air resonance characteristics are shown in Fig.6 for the nominal rotor and airframe inertia configurations.

As with the previously discussed ground resonance results, well-damped higher frequency progressive blade edgewise and flatwise modes were calculated and are omitted for clarity. In contrast, however, for all air resonance cases, an additional unstable very low frequency mode ($\omega < 1$ rad/sec) was calculated. This mode was found to arise from aerodynamic precone related terms and to involve only rigid-body motion of the airframe (elastic blade motions being negligible). For considerations of air resonance stability characteristics and especially in view of the stated purpose of the equation set, this unstable low frequency mode is also omitted from further consideration for clarity.

Figure 6 shows the variations with rotor speed of the frequency and damping characteristics of the three modes of interest: airframe pitch and roll dominant modes, and the blade regressive edgewise dominant mode. Because of the substantial gyroscopic coupling between pitch and roll both the "pitch" and "roll" modes each have significant components of each other. Consequently, because of this coupling and the lower roll inertia, only one instability region was calculated and is roll dominant. Also, in contrast to the ground resonance results, the roll and pitch modes increase in frequency with rotor speed due to the increased flatwise stiffening resulting from increasing centrifugal forces. Note that these results are somewhat simplistic in that throughout the rotor speed variation, aerodynamic thrust as well as blade collective and inflow were maintained at the same levels. Also, no steady flatwise or edgewise bending deflections, with attendant real-world nonlinearities, were introduced.

Again, similar to the above ground resonance results discussion, the remainder of the air resonance results will be presented and discussed only for one rotor speed ($\Omega = 70$ rad/sec). For this rotor speed the principal eigenvalues calculated are as follows:

$$\lambda_{1,2} = -17.127 \pm i30.673$$

$$\lambda_{3,4} = -12.583 \pm i19.325$$

$$\lambda_{5,6} = +0.0622 \pm i26.809.$$

For these air resonance cases the characteristic locus variations were calculated using the unabridged procedure, Eqs.(27) - (30). The results for the nominal airframe inertia and for double the nominal values are shown, respectively, in Figs.7 and 8. Figure 7 clearly shows the instability indicative enclosure of the $(1+i0)$ critical point commensurate with the unstable damping coefficient of $+0.0622$ given above.

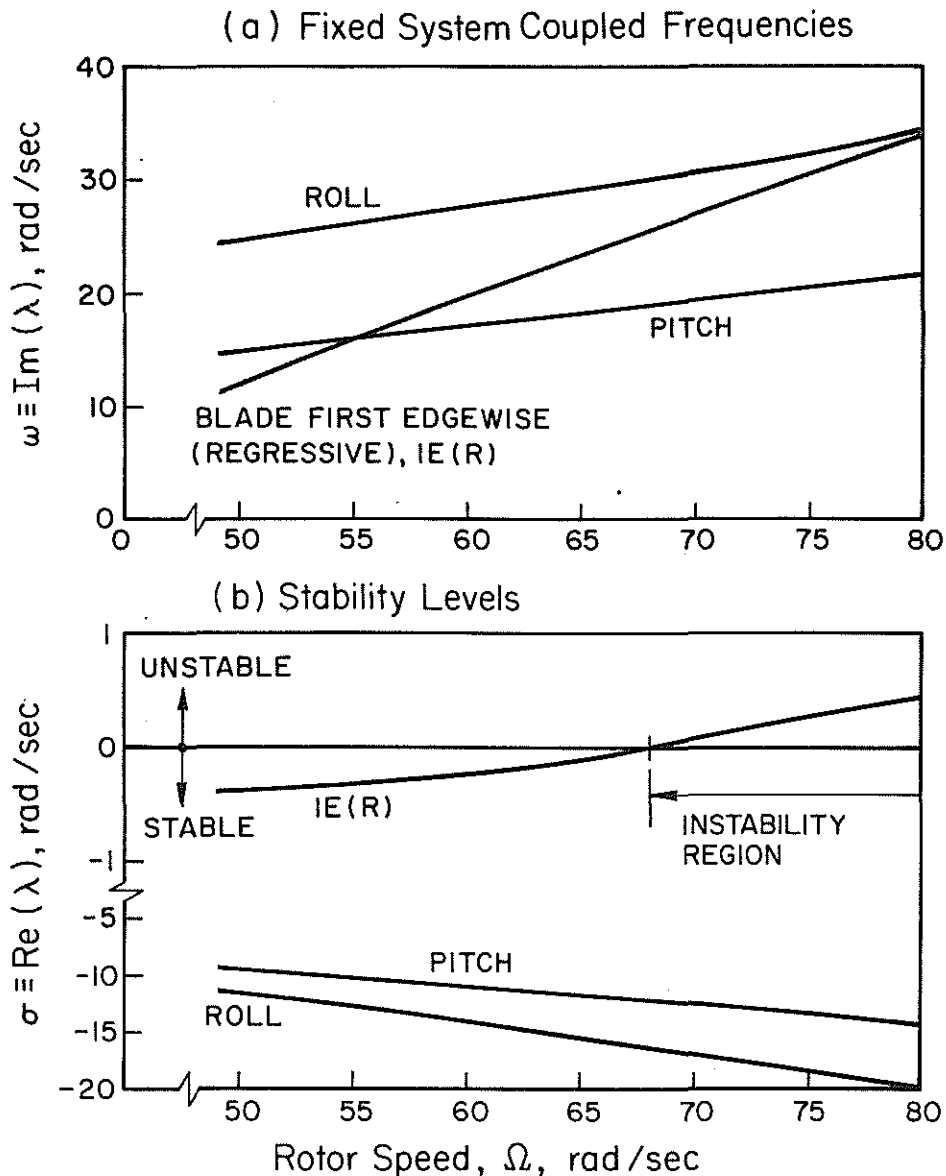


Figure 6 Stability Eigenvalue Variation with Rotor Speed for Nominal Air Resonance Configuration

On the other hand, the results of Fig.8, for an augmented inertia airframe, show nonenclosures of the critical point by the characteristic loci. Indeed, for this case the critical eigenvalue was found to be stable ($\lambda_{\xi, \xi} = -0.0632 \pm i26.620$). It should be stressed that these two sets of results were obtained for the same $G_1(\omega)$ rotor impedance matrix. General features observable from Figs.7 and 8 are (1) the relatively more irregular variability of the characteristic loci with frequency for air resonance compared with that for ground resonance, and (2) the possible multiple crossing of the real axis by one of the characteristic loci. Although no detailed results are presented herein, calculations for a four times airframe inertia configuration showed a very stable critical eigenvalue and no crossings of the positive real axis by any of the characteristic loci.

Lastly, calculations were performed for a constrained airframe configuration wherein the combined system center-of-gravity (.0214 m below the hub) was artificially fixed in space. This constraint effectively reduces

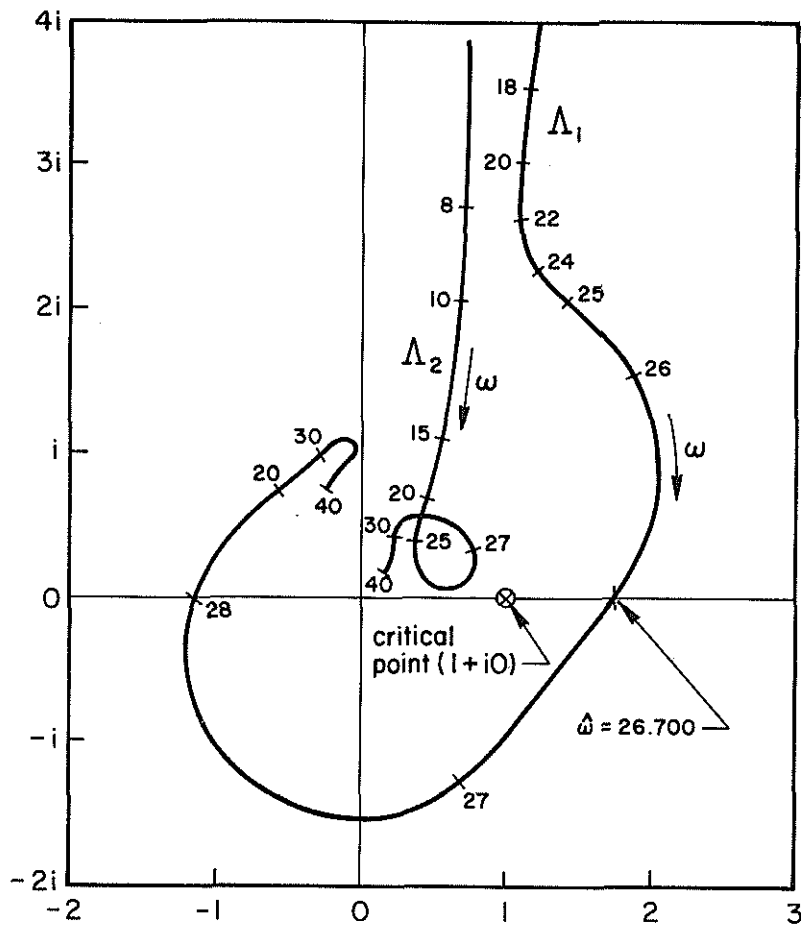


Figure 7 Variations of Principal Characteristic Loci for Nominal Air Resonance Configuration, Condition of Instability, $\Omega = 70$ rad/sec

the dynamic system to a six degree-of-freedom representation. For the nominal and airframe configuration (but with constraint) and a $\Omega = 70$ rad/sec rotor speed the critical eigenvalue was calculated to be $\lambda_{5,6} = 0.100 \pm i26.940$. This represents a 61% error in damping and an 0.5% error in frequency. As expected, the frequency of the constrained system is higher than that for the unconstrained.

Comparison of the results of the eigensolutions with the quantitative stability predictions using the rotor impedance matrix method are presented in Table 3.

These results show the clear success of the rotor impedance method in identifying the instability regions for the completely coupled system for alternate pylon mobilities using the same rotor impedance matrix. In contrast to the ground resonance results, those for the air resonance cases show a marked reduction in the convergence of the approximate eigenvalues to the exact ones.

The exact nature of the convergence properties of these approximate eigenvalues has not yet been fully explored but on the basis of these limited results can be expected to depend on (1) the proximity of the critical characteristic locus to the critical point, (2) the accuracy of the numerical derivatives (which depends on the number and density of points near the critical point), and (3) the degree of Taylor series expansion taken about the critical point.

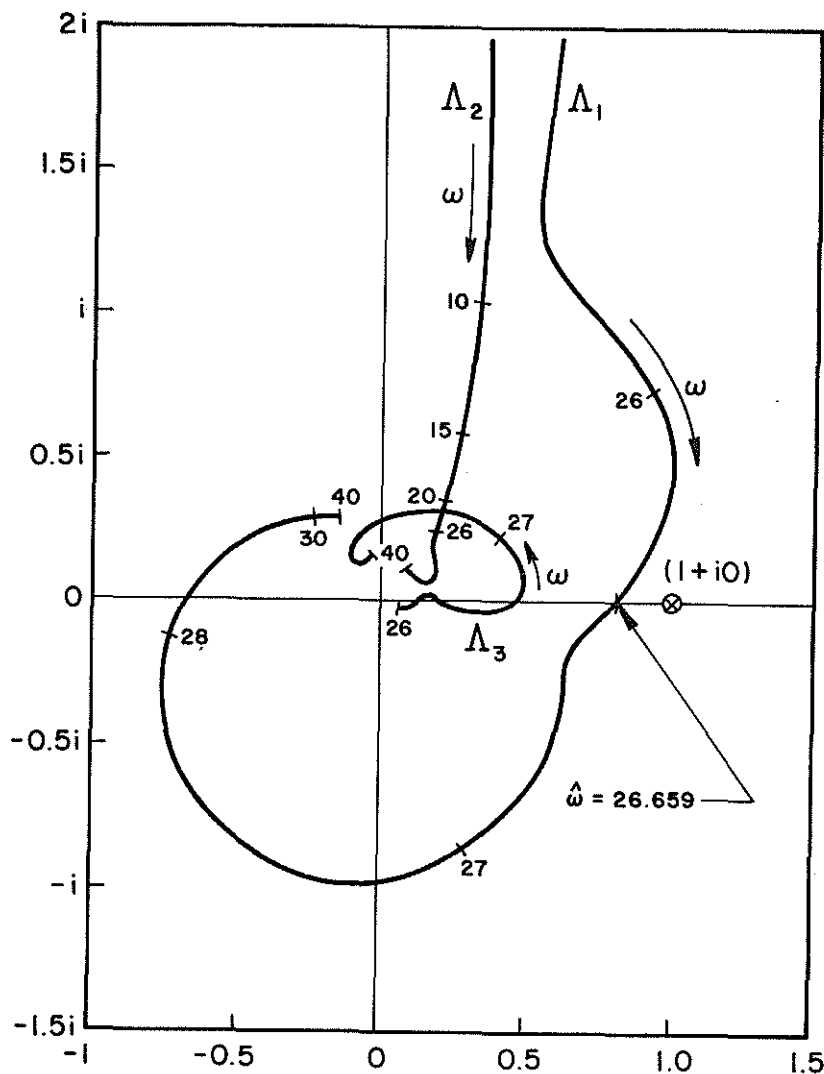


Figure 8 Variations of Principal Characteristic Loci for Augmented Pylon Inertia Air Resonance Configuration, Condition of Stability, $\Omega = 70$ rad/sec

TABLE 3
EIGENVALUE ESTIMATES (AIR RESONANCE)

Pylon Mobility Conditions	$\sigma, \text{Re}(\lambda)$		$\omega, \text{Im}(\lambda)$	
	Value	(% Error)	Value	(% Error)
1. Nominal configuration				
• Actual eigenvalue	0.0622	-	26.809	-
• 1st order approx.	0.1380	121.9	26.800	< 0.1
• 2nd order approx.	0.0338	45.7	26.792	< 0.1
2. Inertias $\times 2$				
• Actual eigenvalue	-0.0632	-	26.620	-
• 1st order approx.	-0.0496	21.5	26.612	< 0.1
• 2nd order approx.	-0.05087	19.5	26.614	< 0.1
3. Constrained				
• Actual eigenvalue	0.100	-	26.940	-
• 1st order approx.	0.163	63.0	26.902	0.1
• 2nd order approx.	0.0538	46.2	26.903	0.1

4. Concluding Remarks

The use of measured rotor impedance characteristics for the testing of coupled helicopter rotor-airframe aeromechanical stability represents a powerful new test methodology. Specific advantages inherent in this new test methodology are:

1. It enables infinite variability of pylon (airframe) parameters from a single rotor impedance test and thus has the potential for greatly increasing the cost-effectiveness of such testing.
2. It relieves the problems attending the design and fabrication of suitably scaled passive pylon masses at model scale.
3. It enables stability testing without the necessity of actually entering the potentially catastrophic instabilities themselves.

On the basis of the results presented herein the following conclusions have been drawn:

1. With regard to the testing for stability boundaries and/or whether the coupled system is stable or not the use of the multivariable Nyquist criterion is a practical tool.
2. The extraction of quantitative stability levels from the characteristic locus characteristics, together with analytic continuation methods, appears to be practical. The convergence characteristics, however, require further study to establish conditions for specified accuracy.
3. The conventional use of artificial constraints on the pylon inertias of scaled, coupled rotor-airframe test models (i.e., using a coincident pitch-roll gimbal) can result in significant errors in stability level measurement.
4. Based on limited analytic approximations the variability of the rotor impedance matrices with frequency can be quite high near one or more rotor resonance conditions. This characteristic has implications for the eventual practical testing of rotors for aeromechanical impedance.

Acknowledgements

The author wishes to acknowledge the useful comments of Dr. J.R. Caspar of United Technology Research Center and the beautiful serenity of the Appalachian Trail which were so instrumental in formulating this work.

References

1. R.E. Donham, S.V. Cardinale and I.B. Sachs, Ground and Air Resonance Characteristics of a Soft In-Plane Rigid Rotor System, Journal of the American Helicopter Society, Vol.14, No.4, October 1969
2. R.T. Lytwyn, W.-L. Miao and W. Woitsch, Airborne and Ground Resonance of Helicopter Rotors, Journal of the American Helicopter Society, Vol.16, No.2, April 1971.
3. W.-L. Miao and H.B. Huber, Rotor Aeroelasticity Coupled with Helicopter Body Motion, Proceedings of the AHS/NASA-Ames Specialists Meeting on Rotorcraft Dynamics, February 1974.
4. D.H. Hodges, Aeromechanical Stability of Helicopters with a Bearingless Main Rotor - Part I, Equations of Motion, NASA TM-78,459, 1978
5. J.A. Staley, R. Gabel and H.I. MacDonald, Full-Scale Ground and Air Resonance Testing of the Army-Boeing Vertol Bearingless Main Rotor, Proceedings of the 35th Annual National Forum of the American Helicopter Society, Paper No.79-23, May 1979.
6. R.T. Lytwyn, Aeroelastic Stability Analysis of Hingeless Rotor Helicopters in Forward Flight Using Blade and Airframe Normal Modes, Proceedings of the 36th Annual National Forum of the American Helicopter Society, Paper No.80-24, May 1980.
7. W.G. Bousman, An Experimental Investigation of the Effects of Aeroelastic Couplings on Aeromechanical Stability of a Hingeless Rotor Helicopter, Proceedings of the 36th Annual National Forum of the American Helicopter Society, Paper No.80-25, May 1980.
8. R.P. Coleman and A.M. Feingold, Theory of Self-Excited Mechanical Oscillations of Helicopter Rotors with Hinged Blades, NACA Technical Report 1351, 1958.
9. W. Warmbrodt, J.L. McCloud III, M. Sheffer and J. Staley, Full-Scale Wind Tunnel Test of the Aeroelastic Stability of a Bearingless Main Rotor, Vertica, Vol.6, pp.165-180, 1982.
10. R.L. Peterson, W. Warmbrodt and J. Hoover, Aeromechanical Stability of a Full-Scale Hingeless Rotor in Hover, Proceedings of the 40th Annual National Forum of the American Helicopter Society, 1984.
11. C.E. Hammond and R.V. Doggett, Determination of Subcritical Damping by Moving Block/Randomec Applications, NASA SP-415, Flutter Testing Techniques Conference Proceedings, pp.59-76, 1976.
12. T.-K. Hsu and D.A. Peters, Coupled Rotor/Airframe Vibration Analysis by a Combined Harmonic Balance, Impedance Matching Method, Journal of the American Helicopter Society, Vol.27, No.1, pp.25-34, January 1982.
13. R. Cansdale, D.R. Gaukroger and C.W. Skingle, A Technique for Measuring Impedance of a Spinning Model Rotor, Royal Aircraft Establishment Technical Report 71092, May 1971.
14. C.J. Savant, Jr., Basic Feedback Control System Design, McGraw-Hill Book Company, Inc., New York, 1958.
15. A.G.J. MacFarlane and I. Postlethwaite, The General Nyquist Stability Criterion and Multivariable Root Loci, International Journal of Control, Vol.25, pp.81-127, January 1977.

16. G.K. Hunt, Similarity Requirements for Aeroelastic Models of Helicopter Rotors, Aeronautical Research Council, CP No.1245, January 1972.
17. F.B. Hildebrand, Introduction to Numerical Analysis, McGraw-Hill Book Company, Inc., New York, 1956.

Nomenclature

a	Airfoil section lift curve slope, 1/deg
b	Number of blades
$[C]$	Hub constraint matrix
C_T/σ	Rotor thrust coefficient per blade solidity
c	Blade chord, cm
c_{d_0}	Airfoil section minimum drag coefficient
c_f	Pylon effective translational damping at hub, N-s/m
EI	Blade bending stiffness, N-m ²
$\{F\}$	Vector of force and moment components at the rotor-pylon interface
F_{x_f}, F_{y_f}	Hub force excitations in x- and y-directions, respectively, N
$[G_1]$	Rotor impedance matrix defining loads per deflections (or accelerations)
$[G_2]$	Pylon mobility matrix defining deflections (or accelerations) per loads
$[H]$	Frequency-dependent dynamic matrix resulting from equations of motion
h_1	Distance airframe c.g. is below rotor hub, m
I_{θ_f}, I_{ϕ_f}	Airframe pitch and roll inertias, respectively, about airframe c.g., kgm ²
k_f	Pylon effective translational stiffness at hub, N/m
l	Characteristic length for scaling purposes, m
M_{x_f}, M_{y_f}	Hub moment excitations in roll and pitch, respectively, N-m
m_f	Airframe (pylon) mass, kg
m_R	Rotor mass, kg
m'	Blade mass distribution, kg/m
R	Rotor radius, m
$S_1, \dots, S_{4\theta}$	Blade mass modal integration constants, as appropriate
T	Rotor thrust, N
$\{X_1\}, \{X_2\}$	Vectors of deflections at respective sides of the artificially disconnected interface
β_B	Blade precone angle, deg
γ	Blade lock number
γ_v, γ_w	Blade 1st edgewise and flatwise bending mode shapes, respectively
e	Value beyond unity that a characteristic locus crosses the real axis
e_x, e_y	Cyclic rotor mode descriptions of blade edgewise bending in longitudinal and lateral directions, respectively
ζ_f	Pylon critical damping ratio used to define damping
ζ_v, ζ_w	Blade structural damping equivalent critical damping ratios for edgewise and flatwise bending, respectively
$\theta_{x_f}, \theta_{y_f}$	Hub roll and pitch motion, respectively, deg
$\theta_{x_R}, \theta_{y_R}$	Cyclic rotor mode descriptions of blade flatwise bending in roll and pitch directions, respectively
$\theta_{\gamma BR}$	Blade collective angle, deg
Λ	Complex-valued characteristic locus
λ	Alternatively, rotor inflow and Laplace transform space eigenvalue ($= \sigma \pm i\omega$), 1/sec

λ_ℓ	Length scale factor
σ	Real part of system eigenvalue, giving stability information, 1/sec
Ω	Rotor speed, rad/sec
ω	Alternatively, frequency variable for impedance and mobility descriptions, and imaginary part of eigenvalue giving coupled frequency information, rad/sec
$\hat{\omega}$	Frequency at which characteristic locus crosses real axis, rad/sec
ω_B	Blade edgewise frequency in rotating coordinate system, rad/sec
ω_f	Natural frequency of arbitrary airframe (pylon) mode with lateral deflection components, rad/s

Superscripts

$()^{(a)}$	Arising from aerodynamic sources
$()^{(p)}$	Arising from motion of pylon mass elements
$()^{(R)}$	Arising from motion of rotor mass elements
$(\bar{ })$	Complex amplitude, from eigensolution or at a discrete frequency
(\sim)	Quantity resulting from application of hub constraint

Subscripts

$()_b$	Blade motion degrees-of-freedom
$()_{FS}$	At full scale
$()_f$	Pertaining to airframe (pylon)
$()_{MS}$	At model scale
$()_p$	Pylon motion degrees-of-freedom
$()_R, ()_I$	Real and imaginary parts, respectively
$()_v, ()_w$	Relating to blade edgewise and flatwise bending, respectively
$()_x, ()_y$	In longitudinal and lateral directions, respectively

Appendix A - Simplified Dynamic Equations for Ground and Air Resonance

The simplified equations of motion presented in this appendix are intended only as a reasonably representative analytical vehicle for evaluating the practicality of the rotor impedance matrix method for testing coupled rotor-pylon instabilities. As such, they are not intended for general analysis applications in support of actual helicopter design efforts. They are presented herein without mathematical development or justification.

The eight differential equations respectively model the responses in hub x- and y-translation, hub roll and pitch rotations, blade cyclic edge-wise bending rotor modes in the x- and y-directions, and blade cyclic flatwise bending rotor modes in roll and pitch directions:

Hub Longitudinal Force (F_x)

$$\begin{aligned}
 & (m_{f_x} + m_R) \ddot{x} + c_{f_x} \dot{x} + k_{f_x} x + (b \beta_B S_{11} - m_{f_1} h_1) \ddot{\theta}_{y_f} \\
 & + \frac{b}{2} \beta_B S_{16} \ddot{\theta}_{y_R} + \frac{b}{2} S_{48} \ddot{\epsilon}_x - T \theta_{y_f} = F_x^{(a)}
 \end{aligned} \tag{A.1a}$$

Hub Lateral Force (F_y)

$$\begin{aligned} & (m_{f_y} + m_R) \ddot{y} + c_{f_y} \dot{y} + k_{f_y} y - (b\beta_B S_{11} - m_{f1} h_1) \ddot{\theta}_{x_f} - \frac{b}{2} \beta_B S_{16} \ddot{\theta}_{x_R} \\ & + \frac{b}{2} S_{48} \ddot{y} + T \theta_{x_f} = F_y^{(a)} \end{aligned} \quad (A.1b)$$

Hub Roll Moment (M_{x_f})

$$\begin{aligned} & - (b\beta_B S_{11} - m_{f1} h_1) \ddot{y} + \left[I_{\varphi_f} + m_{f1} h_1^2 + \frac{b}{2} S_{22} (1 + \beta_B^2) \right] \ddot{\theta}_{x_f} \\ & + \frac{b}{2} S_{12} \ddot{\theta}_{x_R} + 2\Omega \left(\frac{b}{2} \right) S_{22} \dot{\theta}_{y_f} + 2\Omega \left(\frac{b}{2} \right) S_{12} \dot{\theta}_{y_R} \\ & - \beta_B \left(\frac{b}{2} \right) S_{46} \ddot{y} + m_{f1} g h_1 \theta_{x_f} = M_{x_f}^{(a)} \end{aligned} \quad (A.1c)$$

Hub Pitch Moment (M_{y_f})

$$\begin{aligned} & (b\beta_B S_{11} - m_{f1} h_1) \ddot{x} + \left[I_{\theta_f} + m_{f1} h_1^2 + \frac{b}{2} S_{22} (1 + \beta_B^2) \right] \ddot{\theta}_{y_f} \\ & + \frac{b}{2} S_{12} \dot{\theta}_{y_R} - 2\Omega \left(\frac{b}{2} \right) S_{22} \dot{\theta}_{x_f} - 2\Omega \left(\frac{b}{2} \right) S_{12} \dot{\theta}_{x_R} \\ & + \beta_B \left(\frac{b}{2} \right) S_{46} \ddot{x} + m_{f1} g h_1 \theta_{y_f} = M_{y_f}^{(a)} \end{aligned} \quad (A.1d)$$

Rotor Longitudinal Edgewise Excitation (Ξ_{e_x})

$$\begin{aligned} & S_{48} \ddot{x} + \beta_B S_{46} \ddot{\theta}_{y_f} + S_{49} [\ddot{e}_x + 2\zeta_{v_x} \omega \dot{e}_x + (\omega_v^2 - \Omega^2) e_x] \\ & + S_{49} \Omega (2\dot{e}_y + 2\zeta_{v_y} \omega e_x) + \frac{2\beta_B \Omega S_{25}}{25} (\dot{\theta}_{x_R} + \Omega \theta_{y_R}) = \Xi_{e_x}^{(a)} \end{aligned} \quad (A.1e)$$

Rotor Lateral Edgewise Excitation (Ξ_{e_y})

$$\begin{aligned} & S_{48} \ddot{y} - \beta_B S_{46} \ddot{\theta}_{x_f} + S_{49} [\ddot{e}_y + 2\zeta_{v_y} \omega \dot{e}_y + (\omega_v^2 - \Omega^2) e_y] \\ & - S_{49} \Omega (2\dot{e}_x + 2\zeta_{v_x} \omega e_x) + \frac{2\beta_B \Omega S_{25}}{25} (\dot{\theta}_{y_R} - \Omega \theta_{x_R}) = \Xi_{e_y}^{(a)} \end{aligned} \quad (A.1f)$$

Rotor Rollwise Flatwise Excitation ($\Xi_{\theta_{xR}}$)

$$\begin{aligned}
 & - \beta_B S_{1y} \ddot{y} + S_{12} (\ddot{\theta}_{x_f} + 2\Omega \dot{\theta}_{y_f}) + S_{10} [\ddot{\theta}_{x_R} + 2\zeta_{w w} \dot{\theta}_{x_R} + (\omega_w^2 - \Omega^2) \theta_{x_R}] \\
 & + S_{10} \Omega (2\dot{\theta}_{y_R} + 2\zeta_{w w} \theta_{y_R}) - 2\beta_B \Omega S_{25} (\dot{\epsilon}_x + \Omega \epsilon_y) = \Xi_{\theta_{xR}}^{(a)} \quad (A.1g)
 \end{aligned}$$

Rotor Pitchwise Flatwise Excitation ($\Xi_{\theta_{yR}}$)

$$\begin{aligned}
 & \beta_B S_{16} \ddot{x} + S_{12} (\ddot{\theta}_{y_f} - 2\Omega \dot{\theta}_{x_f}) + S_{10} [\ddot{\theta}_{y_R} + 2\zeta_{w w} \dot{\theta}_{y_R} + (\omega_w^2 - \Omega^2) \theta_{y_R}] \\
 & - S_{10} \Omega (2\dot{\theta}_{x_R} + 2\zeta_{w w} \theta_{x_R}) - 2\beta_B \Omega S_{25} (\dot{\epsilon}_y - \Omega \epsilon_x) = \Xi_{\theta_{yR}}^{(a)} \quad (A.1h)
 \end{aligned}$$

where the various integration constants are defined as follows:

$$\begin{aligned}
 S_1 &= \int_0^R m' r \, dr & S_{25} &= R^2 \int_0^R m' \gamma_w \gamma_v \, dr \\
 S_2 &= \int_0^R m' r^2 \, dr & S_{46} &= R \int_0^R m' r \gamma_v \, dr \\
 S_{10} &= R^2 \int_0^R m' \gamma_w^2 \, dr & S_{48} &= R \int_0^R m' \gamma_v \, dr \\
 S_{12} &= R \int_0^R m' r \gamma_w \, dr & S_{49} &= R^2 \int_0^R m' \gamma_v^2 \, dr \\
 S_{16} &= R \int_0^R m' \gamma_w \, dr & & \quad (A.2a-i)
 \end{aligned}$$

Note that this equation set is intended for dual purpose in modeling both ground and air resonance characteristics. For ground resonance applications, only Eqs.(A.1a,b,e,f) are used, with the $()$ terms suppressed. For air resonance applications, all the equations are used, but with the $()$ terms suppressed.

The aerodynamic excitations, indicated by the $()^{(a)}$ superscripted terms on the right-hand side of Eqs.(A.1a-h), were formed using simple quasi-static aerodynamic theory. To this end the static lift curve slope a , a uniform constant drag coefficient c_{d^0} , the collective angle $\theta_{.75R}$, and uniform inflow λ , were included in the formulations. The more realistic effects of twist, air mass dynamics, lift deficiency and nonuniform inflow were omitted consistent with the intended use of the equations. Despite the simplified modeling of these aerodynamics terms, which are more or less standard, their detailed descriptions are sufficiently tedious and insufficiently important to the intent of this paper as to warrant their omission herein.